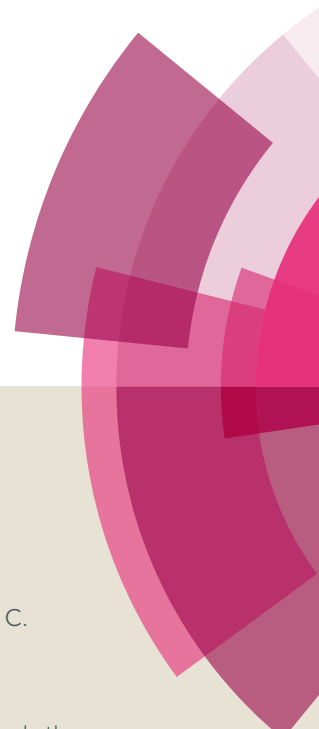


NJC

Accepted Manuscript



This article can be cited before page numbers have been issued, to do this please use: P. T. Gomes, T. C. Cruz, P. M. M. Machado, C. S. B. Gomes, J. R. Ascenso, M. A. N. D. A. Lemos and J. Bordado, *New J. Chem.*, 2018, DOI: 10.1039/C8NJ00350E.



This is an Accepted Manuscript, which has been through the Royal Society of Chemistry peer review process and has been accepted for publication.

Accepted Manuscripts are published online shortly after acceptance, before technical editing, formatting and proof reading. Using this free service, authors can make their results available to the community, in citable form, before we publish the edited article. We will replace this Accepted Manuscript with the edited and formatted Advance Article as soon as it is available.

You can find more information about Accepted Manuscripts in the [author guidelines](#).

Please note that technical editing may introduce minor changes to the text and/or graphics, which may alter content. The journal's standard [Terms & Conditions](#) and the ethical guidelines, outlined in our [author and reviewer resource centre](#), still apply. In no event shall the Royal Society of Chemistry be held responsible for any errors or omissions in this Accepted Manuscript or any consequences arising from the use of any information it contains.

Bis(formylpyrrolyl) cobalt complexes as mediators in the Reversible-Deactivation Radical Polymerization of styrene and methyl methacrylate

Tiago F. C. Cruz,¹ Pedro M. M. Machado,¹ Clara S. B. Gomes,¹ José R. Ascenso,¹
M. Amélia N. D. A. Lemos,² João C. Bordado,² Pedro T. Gomes*¹

¹ Centro de Química Estrutural, Departamento de Engenharia Química, Instituto Superior Técnico, Universidade de Lisboa, Av. Rovisco Pais 1, 1000-049 Lisboa, Portugal;

E-mail: pedro.t.gomes@tecnico.ulisboa.pt

² CERENA, Departamento de Engenharia Química, Instituto Superior Técnico, Universidade de Lisboa, Av. Rovisco Pais 1, 1000-049 Lisboa, Portugal

ABSTRACT: The combination of $[\text{Co}^{\text{III}}\{\kappa^2\text{N},\text{O}-\text{NC}_4\text{H}_3-\text{C}(\text{H})=\text{O}\}_2(\text{PMe}_3)_2]$ (**1**) and tert-butyl- α -bromoisobutyrate (tBiB-Br) is a suitable initiation system for controlling the radical polymerization of styrene, by an Atom Transfer Radical Polymerization (ATRP) mechanism, below 70 °C and of methyl methacrylate, by an Organometallic Mediated Radical Polymerization (OMRP)/Catalytic Chain Transfer (CCT) interplay mechanism, below 50 °C. The pure ATRP nature of styrene polymerization allowed the synthesis of the polystyrene-*b*-poly(methyl methacrylate) block copolymer, as confirmed by GPC/SEC and DOSY NMR studies. Attempts to isolate a Co(III) species containing a Br atom (**Co(III)-Br**), supposedly a key ATRP deactivator, by reacting **1** and tBiB-Br quantitatively afforded the cationic Co(III) complex $[\text{Co}^{\text{III}}\{\kappa^2\text{N},\text{O}-\text{NC}_4\text{H}_3-\text{C}(\text{H})=\text{O}\}_2(\text{PMe}_3)_2]\text{Br}$ (**2**). Metathetic exchange reactions of complex **2** with TIX gave rise to analogues of the type $[\text{Co}^{\text{III}}\{\kappa^2\text{N},\text{O}-\text{NC}_4\text{H}_3-\text{C}(\text{H})=\text{O}\}_2(\text{PMe}_3)_2]\text{X}$ (**3a**, X=BF₄⁻; **3b**, X=BPh₄⁻), containing non-coordinating anions. In the absence of a radical initiator, complex **2** mediated the formation of polystyrene and poly(methyl methacrylate), with poor control, likely via a Generation of Activators by Monomer Addition (GAMA) mechanism. Complexes **3a** and **3b**, however, have shown to be completely inactive. Addition of 0.5 equivalents of AIBN to **2**, drastically improved the molecular weight control in the polymerization of styrene, at 70 °C, through a reverse-ATRP mechanism.

Keywords: Reversible-Deactivation Radical Polymerization (RDRP), Atom Transfer Radical Polymerization (ATRP), Catalytic Chain Transfer (CCT), polystyrene, poly(methyl methacrylate), formylpyrrolyl ligands

Introduction

Reversible-deactivation radical polymerizations (RDRP) is a set of powerful tools to obtain well-defined polymeric architectures leading to important applications in materials science and technology. RDRP allows the synthesis of polymers with a predetermined molecular weight and precise molecular weight distributions under mild reaction conditions.¹ RDRP processes are versatile enough to control polymer topology, composition and chain-end functionality. The control in RDRP arises from rapid initiation and minimization of chain-breaking reactions, such as chain transfer or undesired termination, by establishing an equilibrium between the propagating radicals and dormant species.² RDRP processes can occur via Reversible Transfer (RT) or Degenerative Transfer (DT). In RDRP by RT, a radical species is involved in the activation/deactivation equilibrium of the propagating polymeric chain.^{2,3} A particular case of RDRP by RT is Atom Transfer Radical Polymerization (ATRP). In an ATRP process, an organometallic/coordination compound is involved in an equilibrium with a halogen atom by means of a redox process, via quick protection/deprotection of the polymeric propagating chain.^{4,5} In RDRP by DT the control is possible due to a transfer agent, by means of a transfer group.²

Whenever coordination/organometallic species are involved in RDRP, and the control throughout the polymerization is based on the reversible homolytic cleavage of a metal-carbon alkyl bond,^{6,7} the process is called Organometallic Mediated Radical Polymerization (OMRP).⁸ An important phenomenon to point out is Catalytic Chain Transfer (CCT), occurring when an organoradical, either *per se* or when stabilized by an organometallic deactivator, undergoes β -hydrogen transfer reactions.⁹ CCT is likely dependent on the degree of stereochemical hindrance and electronic effects induced by the coordination sphere of the metal complex and, more importantly, on the nature of the monomer.¹⁰

The field of Cobalt Mediated Radical Polymerization (CMRP)¹¹ has its origin in the use of organocobalt(III) complexes to generate carbon-centred radicals, owing to the facile Co-C homolysis, and to their propensity in exhibiting the persistent radical effect. By Co-R homolytic cleavage, a one electron transformation occurs,¹² leading to a carbon-centred radical R[•] that initiates polymerization, and a cobalt(II) complex that acts as a persistent radical, being present in the activation/deactivation equilibrium of RDRP. By these reasons, and taking into account the properties of vitamin B12 complexes,¹³ porphyrinic Co(III) complexes have been part of the early systems in CMRP, as pointed out in the seminal work of Wayland *et al.*,¹⁴ being one of the most studied class of examples (Chart 1, A).¹⁵ Generally, molecular weight control is optimal when steric

hindrance is high, because CCT is minimized. It was also found that increasing the donating character of R substituents helps the controllability, since the equilibrium is shifted to the dormant polymeric species, while the activity decreases. Complexes with sulfonated ligands have been used for acrylic acid polymerization in aqueous media, giving rise to dispersities ($\bar{D} = M_w/M_n$) as low as 1.2.¹⁶

Bis(ketiminato) cobalt complexes have also been widely studied (Chart 1, **B**), especially for the polymerization of vinyl acetate, producing polymers with \bar{D} as low as 1.1.¹⁷ In light of several DFT studies, bis(acetylacetonate) complexes of the type $\text{Co}(\text{acac})_2\text{L}_2$ (with L being pyridine, tetrahydrofuran, dimethylsulfoxide or N,N-dimethylformamide, and acac being the acetylacetonate ligand) have been developed (Chart 1, **C**),^{18–21} leading to very active and controlled systems for a wide range of vinyl monomers.¹¹ Also in this case, the electron donating groups and the chelation effect of the monomer improve the molecular weight control through the stabilization of the metal mediator (the $\text{Co}(\text{acac})_2$ moiety).²² Aside from these quite explored examples, cobaltocene has been applied in the ATRP of methyl methacrylate, leading to dispersities of 1.2.²³

Our group has been involved in the synthesis and reactivity studies of cobalt complexes of bidentate *N,N*-iminopyrrolyl and *N,O*-ketopyrrolyl ligands.^{24,25} We have reported previously the synthesis and characterization of the paramagnetic 19-electron complex $[\text{Co}^{\text{III}}\{\kappa^2\text{N},\text{O}-\text{NC}_4\text{H}_3-\text{C}(\text{H})=\text{O}\}_2(\text{PMe}_3)_2]$ (Chart 1, **1**),²⁵ which will now serve as the starting point of the present study, owing to its resemblance with some of the $\text{Co}(\text{acac})_2\text{L}_2$ mediators mentioned above. Therefore, in this work, we present the first case of ketopyrrolyl cobalt RDRP mediation of styrene (Sty) and methyl methacrylate (MMA), and attempt to obtain mechanistic insights into its behaviour.

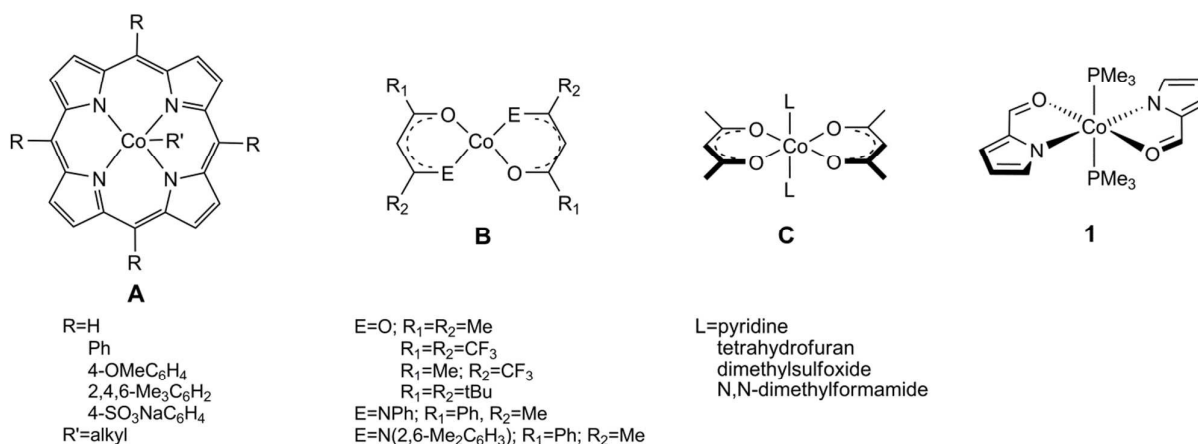


Chart 1 Several cobalt-based compounds studied in RDRP: porphyrinic complexes (**A**), ketiminato and acetylacetonate derivatives (**B**, **C**) and the complex of the present work (**1**).

Results and Discussion

Homopolymerizations of styrene and methyl methacrylate mediated by complex 1 – ATRP conditions:

In order to work under ATRP conditions, complex 1 was combined with t-butyl- α -bromoisobutyrate (tBiB-Br). The system 1/tBiB-Br was very active in the polymerization of Sty and MMA, at temperatures ranging from 50 to 90 °C, and [monomer]:[1]:[tBiB-Br] ratios between 100:1:1 and 1000:1:1. No activity for this system was observed below 50 °C for Sty, and below 25 °C for MMA. Similarly, no activity was observed in the absence of either 1 or tBiB-Br (Sty auto-initiation, observed at 90 °C, never exceeded 5% conversion). Figure 1 depicts the kinetics of polymerization at different temperatures for Sty and MMA (see also Table S1 in ESI). The polymerization of MMA (Figure 1a) always proceeded with a higher activity than that of Sty (Figure 1b), but both cases follow a first order behaviour in Sty or in MMA. As expected, the activity increased with increasing temperatures and higher monomer concentrations.

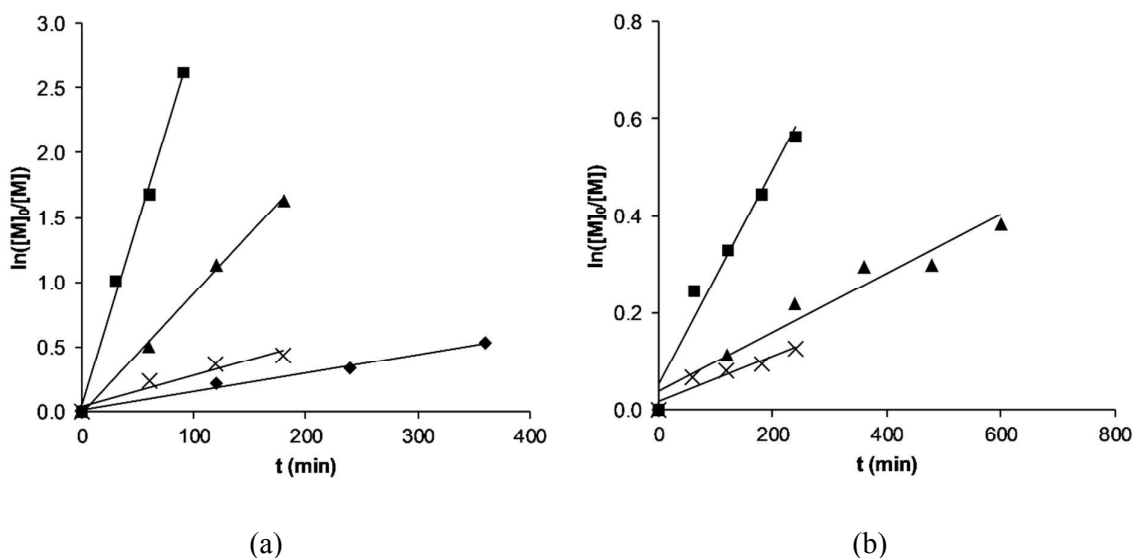


Figure 1 First order kinetic plots ($\ln([M]_0/[M])$ vs. time) for the homopolymerizations of MMA (a) and Sty (b), at 90 (squares), 70 (triangles), 50 (crosses) and 25 °C (diamonds). [Monomer]:[1]:[tBiB-Br]=500:1:1; $V_{\text{monomer}}:V_{\text{toluene}}=5:5$ mL.

The plots of the number-average molecular weights (M_n) of the homopolymers obtained, determined by Gel Permeation Chromatography/Size-Exclusion Chromatography (GPC/SEC), versus the monomer conversion are represented in Figure 2 and show that the temperature plays an important role. The system 1/tBiB-Br behaves relatively close to ideal at 50 °C in the polymerization of MMA (Figure 2a), and below 70 °C for the polymerization of Sty (Figure 2b),

whereby the experimental molecular weights are close to the theoretical living polymerization line ($M_n = \{[M]/[tBiB-Br]\} \times \text{conv}$).

In the case of MMA polymerization, the molecular weights are lower than the ones predicted by the living polymerization line and this effect is more pronounced with increasing temperatures, which is a consequence of a chain transfer-dominated polymerization. The \bar{D} values always lie between 1.6 and 1.2. The molecular weights lie lower than expected even for the best results for the MMA polymerization (at lower conversions). Owing to the modest molecular weight control exhibited in these polymerization reactions, additional experiments utilizing AIBN alone or **1**/AIBN as radical initiators were performed (see Table S2 of the ESI). The polymerization of MMA using **1**/AIBN yielded polymers with molecular weights 1.1 to 1.7 times higher than the ones obtained by mediation with **1**/tBiB-Br (likely due to a non-quantitative decomposition of AIBN). However, the molecular weights obtained with the **1**/AIBN system are still dramatically lower (27 to 32 times lower) than those of the MMA polymerization with AIBN alone (classical free radical polymerization conditions).

In Sty polymerization, the molecular weights lie closer to the ideal case, however having the tendency do increase at higher conversions for reactions at higher temperatures, indicating the minimization of unwanted termination reactions. The range of \bar{D} values is between 1.8 and 1.3.

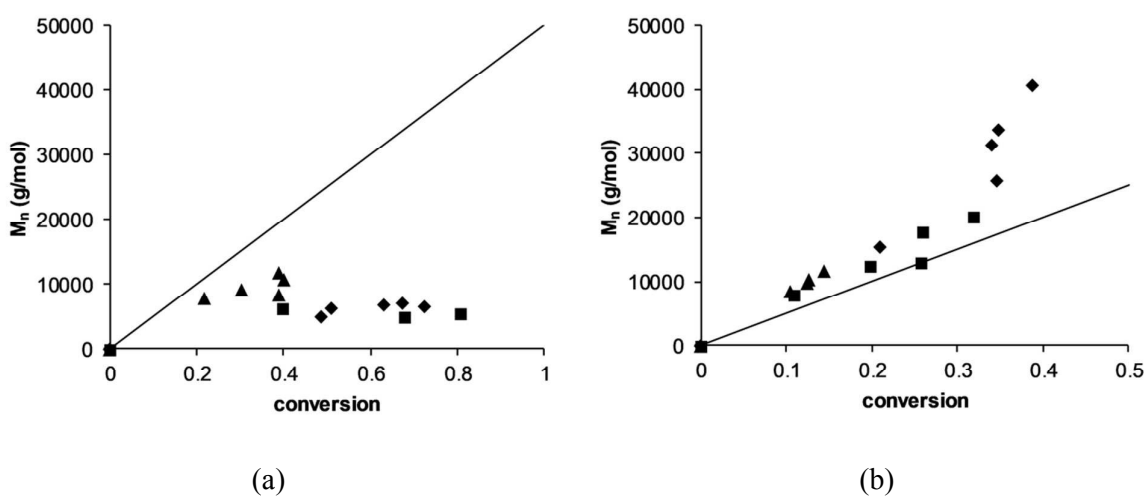


Figure 2 Plots of molecular weight vs. conversion of MMA (a) and Sty (b), at 90 (diamonds), 70 (squares), 50 (triangles) °C. [Monomer]:[**1**]:[tBiB-Br]=500:1:1; $V_{\text{monomer}}:V_{\text{toluene}}=5:5$ mL. The straight lines represent the theoretical living polymerization M_n values.

The homopolymerization reactions involving complex **1** were also performed in 1,2-dichloroethane or THF, from which no significant additional kinetic or molecular weight control effects have been observed with respect to the reactions performed in toluene.

The ^1H NMR spectra of the polystyrene (PS) samples obtained with controlled molecular weights (Figure 3 (top)) display typically broad resonances and show atactic stereochemical configurations ($P_r \approx 0.5$). They also show a minor resonance at 4.7–4.5 ppm, corresponding to a terminal methine proton (H^3 in Figure 3 (top)) of a bromine terminated polystyrene (PS-Br).²⁶ The ^1H NMR of the poly(methyl methacrylate) (PMMA) formed under molecular weight controlled conditions (Figure 3 (bottom)) are typical of a highly syndiotactic-rich polymer ($P_r > 0.7$), expected for a radical polymerization.²⁷ Furthermore, the ^1H NMR spectra of the PMMA samples consistently show two minor resonances, between 6.3 and 5.3 ppm, corresponding to the two geminal protons of the vinyl end-group generated by β -hydrogen transfer reactions, and, between 2.6 and 2.3 ppm, corresponding to the allyl protons of the same end-group.²⁸

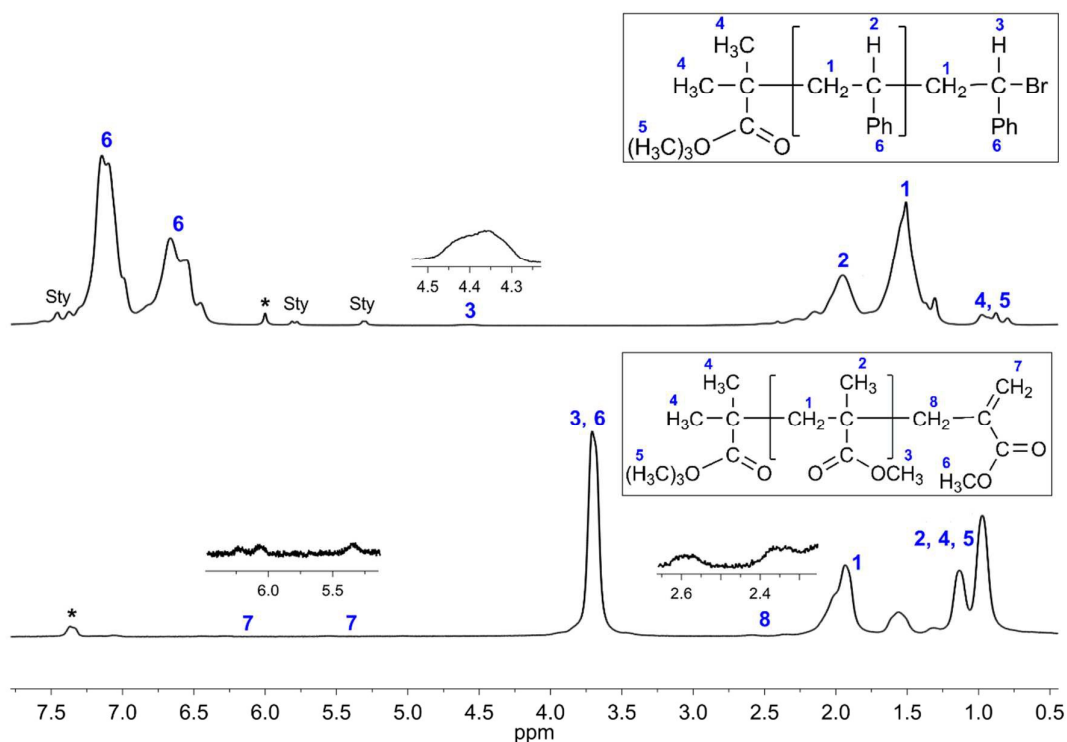


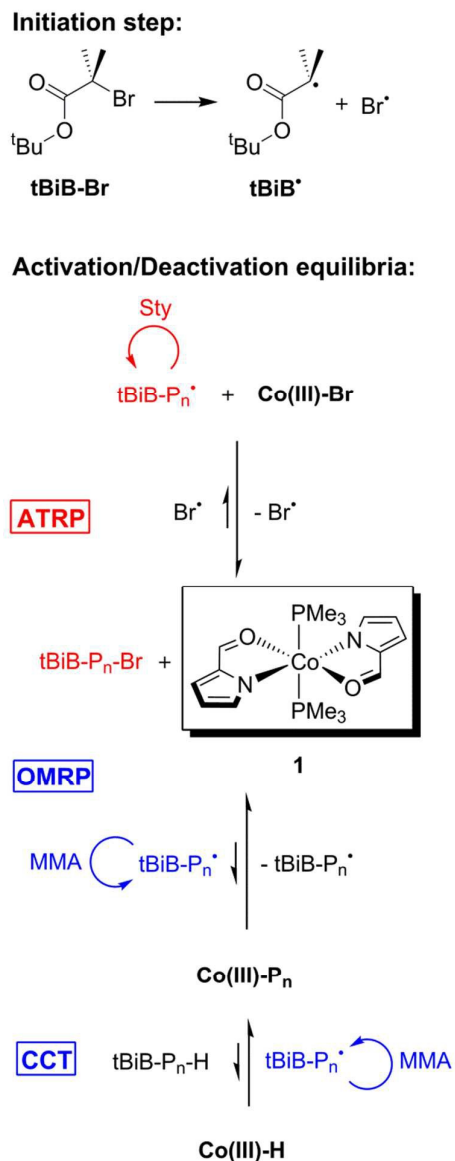
Figure 3 Stacking of typical ^1H NMR spectra of the PS (top) (300 MHz, in 1,1,2,2-tetrachloroethane- d_2 (*), at 120 °C) and of the PMMA (bottom) (300 MHz, in CDCl_3 (*), at 55 °C). [Monomer]:[**1**]:[tBiB-Br]=500:1:1; $V_{\text{monomer}}:V_{\text{toluene}}=5:5$ mL; reaction temperature: 70 °C for PS, and 50 °C for PMMA.

Aside from NMR spectroscopy and GPC/SEC, selected polymer samples were analyzed by MALDI-TOF mass spectrometry. In the case of styrene, inconclusive results were obtained owing to the systematic failure in ionizing the respective samples. This property has been specifically reported for bromine-terminated polystyrenes.²⁹ In the case of the analyzed PMMA samples (see Figures S1 and S2 of the ESI), the lower molecular weight fractions revealed the absence of bromine-terminated PMMA.

These observations indicate that, under ATRP conditions, the system behaves differently, depending on the monomer.

Mechanistically wise, in the case of MMA, although initiation occurs through homolytic cleavage, a Br termination could not be observed, ruling out an ATRP mediation. Additionally, chain transfer reactions via β -hydrogen transfer of the PMMA chains are highly favoured, being this process intensified at higher conversions and temperatures. For this reason, we propose that the activation/deactivation process occurs via a OMRP/CCT interplay mechanism, whereby complex **1** is a persistent radical and reversibly protects to a certain extent the polymeric radicals (species **Co(III)-P_n** in Scheme 1), as evidenced by the experiments using **1**/AIBN as mediator. This type of mechanism interplay has been observed before, the first report by Poli *et. al.* using half sandwich Mo(III)/Mo(IV) complexes.³⁰

For the polymerization of Sty, other conclusions can be drawn. At higher temperatures and conversions, recombination reactions and contamination effects from thermal initiation are favoured (some PS GPC/SEC chromatograms at higher temperatures and conversions show bimodal distributions), justifying the poorer control. At lower temperatures, termination reactions are drastically minimized, occurring exclusively due to recombination with the bromine radical. Polystyrenes with brominated end-groups are thus synthesized. Therefore, it is postulated that styrene polymerization occurs via a pure ATRP mechanism, with the initiation of the polymerization occurring by homolytic cleavage of tBiB-Br (Scheme 1), whereby a Co(III) complex containing a Co-Br bond (**Co(III)-Br**) works as the radical chain deactivator species of the polymerization process, being involved in a bromine atom transfer equilibrium with the radical growing chain.



Scheme 1 Proposed mechanisms for the homopolymerizations of Sty (ATRP) and MMA (OMRP/CCT).

Polymerization of MMA with a PS-Br macroinitiator mediated by complex 1 – synthesis of a PS-*b*-PMMA block copolymer: Complex 1 combined with the previously synthesized PS-Br macroinitiator successfully yielded a PS-*b*-PMMA block copolymer, in a polymerization reaction with MMA. This polymerization reaction proceeded in a controlled manner (Figure 4a – see also Table S1 of the ESI), at 50 °C, with an increase of the molecular weights and decrease of the Đ values with conversion, varying from 1.76 to 1.36. The rate of this polymerization was lower than the one of the corresponding MMA homopolymerization with the 1/tBiB-Br system. All of the GPC/SEC chromatograms obtained throughout the copolymerization reaction correspond to monomodal distributions and show lower retention times than those of the corresponding

macroinitiator (Figure 4b). This indicates a successful chain extension of the polystyryl block with methyl methacrylate units.

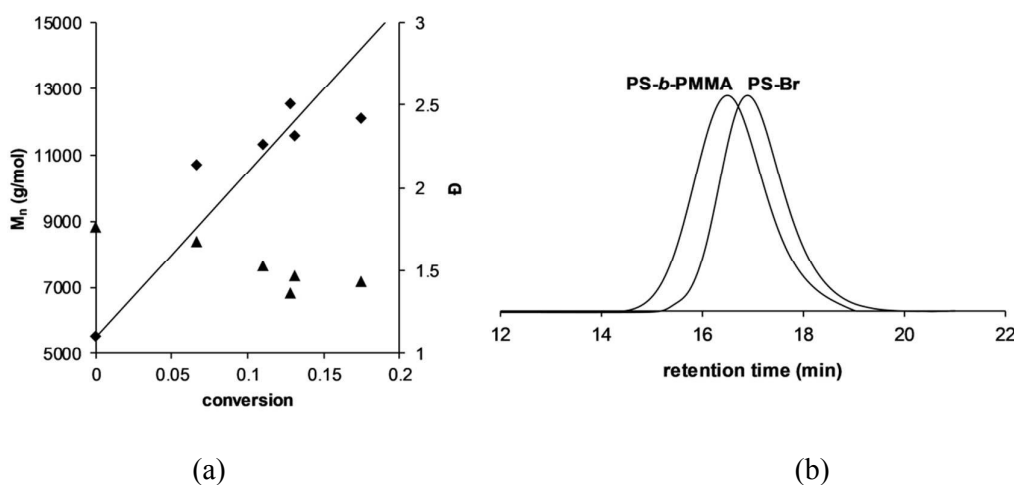


Figure 4 (a) Plots of molecular weight (diamonds) and dispersity (triangles) vs. the MMA conversion throughout the copolymerization reaction (the straight line represents the theoretical living polymerization M_n values); (b) GPC/SEC chromatograms of the PS-*b*-PMMA block copolymer (M_n=12600 g mol⁻¹, Đ=1.36) and the brominated PS macroinitiator, PS-Br (M_n=5500 g mol⁻¹, Đ=1.76). [MMA]:[I]:[PS-Br]=500:1:1; reaction temperature: 50 °C.

The ¹H NMR spectrum of the copolymer shows the expected resonances corresponding to both polystyryl and poly(methyl methacrylate) blocks and the disappearance of the characteristic resonance of a brominated polystyrene (see Figure S3 in ESI). The ratio of styrenic to methyl methacrylate units is 1:1.69. The stereochemistries of the two blocks are similar to those observed in the respective homopolymers.

To complement these results, Diffusion Ordered Spectroscopy (DOSY) NMR experiments were performed. In the DOSY NMR spectrum of the block copolymer (Figure 5) it is possible to observe that all of the styrenic and methyl methacrylate moieties have a single diffusion coefficient (D) of 6.97×10⁻¹⁰ m² s⁻¹, showing that, despite the difference in the structural natures of the two blocks, a single entity is present in solution, thus confirming the presence of a true copolymer and not a mixture of homopolymers.

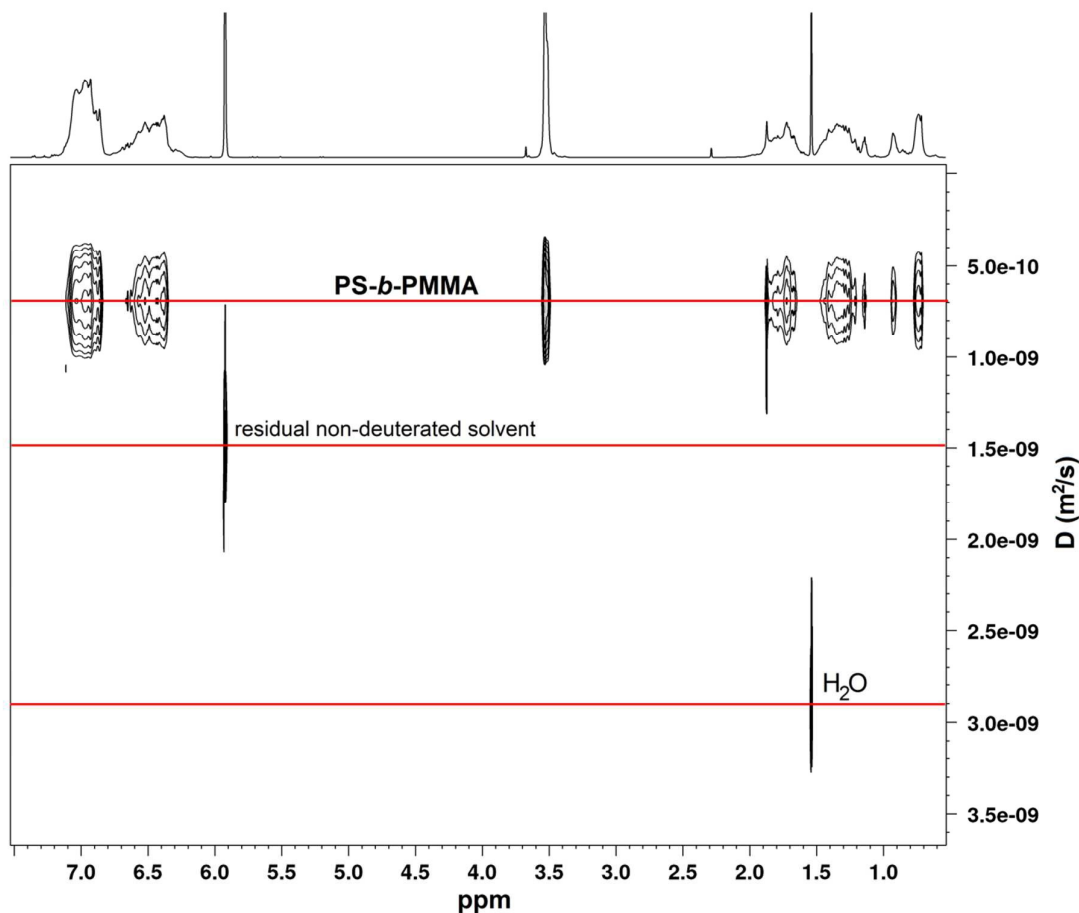
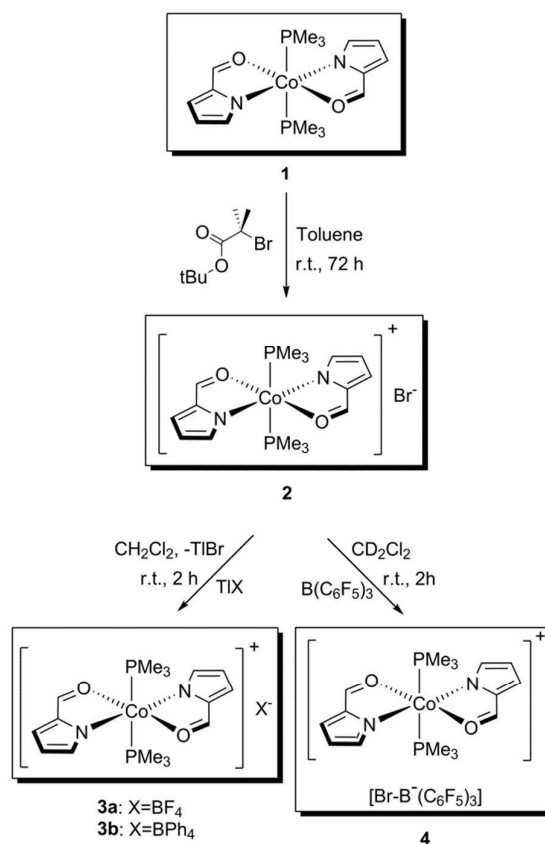


Figure 5 DOSY NMR spectrum of the PS-*b*-PMMA block-copolymer (500 MHz, in 1,1,2,2-tetrachloroethane- d_2 , at 25 °C).

Attempts to isolate the ATRP cobalt radical chain deactivator species: In an attempt to isolate the complex species **Co(III)-Br**, proposed as a key species in the activation/deactivation equilibrium of an ATRP process (see Scheme 1), the stoichiometric reaction of **1** and tBiB-Br was performed. From a brown-yellow toluene solution of **1** and one equivalent of tBiB-Br, an orange solid gradually precipitated. Washing of the resulting solid with toluene and recrystallization from dichloromethane/*n*-hexane gave rise to the diamagnetic cationic complex $[\text{Co}^{(\text{III})}\{\kappa^2\text{N},\text{O}-\text{NC}_4\text{H}_3-\text{C}(\text{H})=\text{O}\}_2(\text{PMe}_3)_2]\text{Br}$ (**2**) in a nearly quantitative yield (Scheme 2), possibly with concomitant formation of organic products resulting from the recombination and/or disproportionation tBiB• radicals. This cationic Co(III) complex is derived from the one-electron oxidation of **1** by tBiB-Br, whilst maintaining its coordination sphere, and a bromine being present as the counter-anion. Treatment of a dichloromethane solution of **2** with the thallium salts (TlBF₄ or TlPh₄) smoothly afforded quantitatively the complexes $[\text{Co}^{(\text{III})}\{\kappa^2\text{N},\text{O}-\text{NC}_4\text{H}_3-\text{C}(\text{H})=\text{O}\}_2(\text{PMe}_3)_2]\text{X}$ (X=BF₄⁻ (**3a**), B(C₆H₅)₄⁻ (**3b**)), by metathetic exchange of the bromine counter-anion by tetrafluoroborate and

tetraphenylborate anions, respectively, with precipitation of thallium bromide (Scheme 2). Complexes **2**, **3a** and **3b** are insoluble in *n*-hexane, toluene, diethyl ether and THF and are soluble in dichloromethane. These complexes are relatively stable to air, since they readily crystallized from dichloromethane solutions exposed to air. This contrasts with the air sensitivity of complex **1**, particularly in solution.



Scheme 2 Attempts to isolate a **Co(III)-Br** radical chain deactivator species in the ATRP system **1**/tBiB-Br.

The isolation of **2** did not afford the expected Co(III) complex containing a coordinated Br⁻ ligand. A further attempt to trap such species, which is labelled as **Co(III)-Br** (Scheme 1), involved the NMR-scale stoichiometric reaction of **2** and B(C₆F₅)₃ in CD₂Cl₂. However, the expected abstraction of a PMe₃ ligand by B(C₆F₅)₃ to give the neutral adduct (C₆F₅)B←PMe₃ did not occur, as no precipitate was observed in the reaction medium.³¹ Instead the formation of the cationic complex [Co^(III){κ²N,O-NC₄H₃-C(H)=O}₂(PMe₃)₂][BrB(C₆F₅)₃] (**4**) took place, which contains the same cationic moiety of compound **2** and the bromotris(pentafluorophenyl)borate anion resulting from the addition of the Br⁻ counter-anion of **2** to B(C₆F₅)₃.

Complexes **2**, **3a**, **3b** and **4** are formally 18-electron diamagnetic species and were characterized by NMR spectroscopy. The ^1H NMR spectra of these compounds feature the expected resonances for the formylpyrrolyl moiety and an intense triplet around 0.8 ppm, indicating the presence of two trimethylphosphine for two formylpyrrolyl ligands. In addition, complex **3c** also shows the expected resonances for the tetraphenylborate counter-anion. The resonance corresponding to the trimethylphosphine protons is a triplet ($^2J_{\text{HP}}=6$ Hz), which is characteristic of a proton-phosphorous virtual coupling in a complex displaying a phosphorus-metal-phosphorus *trans* arrangement.³² The $^{13}\text{C}\{^1\text{H}\}$ NMR spectra of these complexes display the expected resonances, showing the same coupling pattern as far as the trimethylphosphine moiety is concerned – a triplet consistent with a carbon-phosphorus *trans* virtual coupling ($^2J_{\text{CP}}=13.5$ Hz). It is also possible to observe long range carbon-phosphorous couplings of the C3 and C5 carbons of the pyrrolyl moiety, as they also appear as triplets, albeit with much smaller coupling constants. The $^{31}\text{P}\{^1\text{H}\}$ spectra of these complexes show a singlet resonance at *ca.* 13 ppm, in accordance to similarly reported compounds.³³ The $^{11}\text{B}\{^1\text{H}\}$ resonances of complexes **3a**, **3b** and **4** appear between 0 and -7 ppm, respectively, falling in the range of borate anions.³⁴

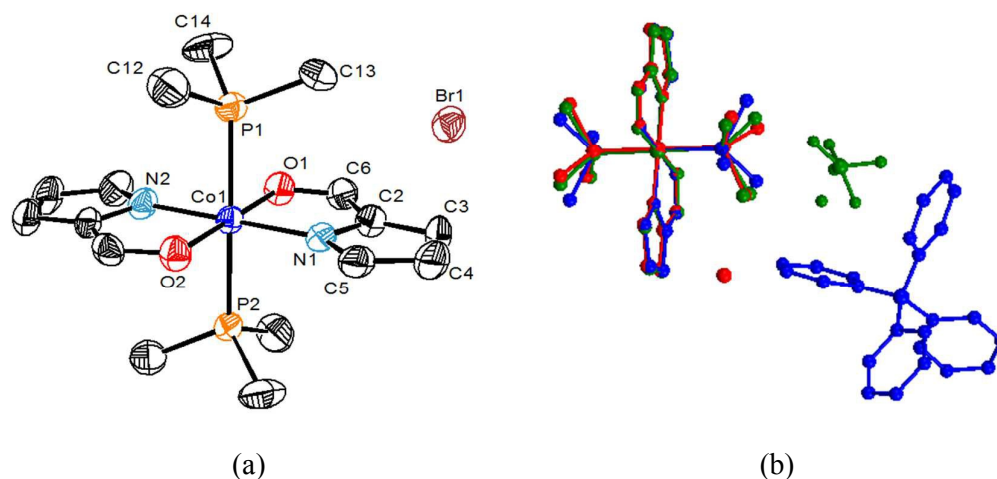


Figure 6 (a) ORTEP-3 diagram of the X-ray diffraction structure of molecule **2**, showing 50% probability ellipsoids, with hydrogen atoms omitted for clarity. (b) Ball and stick representation of the superimposed X-ray diffraction structures of complexes **2** (red), **3a** (green) and **3b** (blue), with hydrogen atoms and solvate molecules omitted for clarity, showing the close equivalence between the cationic moieties of the three complexes.

Complexes **2**, **3a** and **3b** were also characterized by X-ray diffraction. Selected bond distances and angles are listed in Table 1, and the crystallographic data and a detailed selection of bond parameters are presented in Tables S5 and S6 of the ESI, respectively. Complexes **2**, **3a** and **3b** crystallized in the orthorhombic, monoclinic and triclinic system, respectively. Complex **2** and **3b**

co-crystalized with one water and one dichloromethane molecule in the asymmetric unit, respectively. Complex **3b** has two half cationic molecules with each Co atom corresponding to 50% occupancy.

Table 1 Selected bond distances and angles for complexes **2**, **3a** and **3b**

	2		3a	3b	
	Ligand 1	Ligand 2		Ligand 1	Ligand 2
<i>Distances (Å)</i>					
Co(1)-N(1)	1.899(4)	1.901(4)	1.898(2)	1.898(2)	1.898(2)
Co(1)-O(1)	1.921(4)	1.928(4)	1.912(2)	1.9199(19)	1.9219(19)
Co(1)-P(1)	2.2827(18)	2.2820(18)	2.2793(11)	2.2762(7)	2.2709(7)
O(1)-C(6)	1.271(6)	1.262(6)	1.285(5)	1.285(4)	1.282(3)
<i>Angles (°)</i>					
N(1)-Co(1)-O(1)	83.65(17)	83.74(18)	84.18(10)	84.73(9)	84.13(9)
O(1)-Co(1)-P(1)	88.38(12)	88.51(12)	89.12(9)	87.83(6)	87.95(6)
N(1)-Co(1)-P(1)	90.91(14)	90.17(14)	90.08(9)	89.53(7)	87.73(7)

The ORTEP-3 diagram of complex **2** is presented in Figure 6a. Since the Co(III) cationic units in the three complexes are very similar, Figure 6b shows a superimposition of their ball and stick representations. In all three complexes, the two trimethylphosphine ligands adopt a *trans* conformation and the two bidentate formylpyrrolyl ligands are *transoid* in an almost octahedral geometry around the metal centre: the N(1)-Co(1)-P(1) and O(1)-Co(1)-P(1) bond angles fall between 87.73(7) and 90.91(14) degrees for all three complexes, and the N(1)-Co(1)-O(1) bite angles lie between 83.65(17) and 84.73(9) degrees. The Co(1)-P(1), Co(1)-N(1) distances lie in the range 2.2709(7)-2.2827(18) Å and 1.898(2)-1.901(4) Å, respectively, which are in accordance with the values reported for Co(II) or Co(III) complexes containing ketopyrrolyl ligands.^{25,33} These values are quite analogous to the ones reported by our group for the low-spin ($S = 1/2$) Co(II) precursor complex **1**,²⁵ which is isostructural with **2**, **3a** and **3b**, observation that can also be extended to the formylpyrrolyl ligand bond parameters in this type of Co complexes.^{25,33} The positive charge of the oxidized 18-electron Co(III) complexes is then compensated by the respective counter-anion. The striking difference between precursor **1** and complexes **2**, **3a** and **3b** lies in the Co1-O1 bond distance, which is considerably longer in complex **1** (2.3854(15) Å) than in complexes **2**, **3a** and **3b** (1.912(2)-1.928(4) Å). The latter values are in accordance with previously reported Co(III) complexes featuring the ketopyrrolyl moiety.³³ The shortening of the Co1-O1 bond length is due to the formal loss of one electron – a Co(II) to Co(III) oxidation – from the d_{2^2} -based

antibonding SOMO orbital of the Co(II) complex **1**, which becomes empty,²⁵ thus generating an electronically saturated and a more electrophilic metal centre.

Cyclic voltammetry studies of complexes 1, 2 and 3a: Complexes **1**, **2** and **3a** were studied by cyclic voltammetry (CV) in dichloromethane solution, using $[N(n\text{-Bu})_4][\text{BF}_4]$ as a supporting electrolyte, in order to evaluate their redox behaviour. The cyclic voltammograms are presented in Figure 7 and the respective redox peaks are listed in Table 2. The cyclic voltammetry of the paramagnetic 19-electron complex **1** shows a one electron oxidation process at -0.03 V vs. SHE corresponding to the oxidation of Co(II) to Co(III) displaying an approximately 2 fold increase in the current-function ($i_{p_{\text{ox}}} / ([\mathbf{1}] \times \sqrt{v})$; where $i_{p_{\text{ox}}}$ is the oxidation peak intensity and v is the scan rate) for a 50 fold decrease in the scan rate (Figure S8 of the ESI). This behaviour indicates that the oxidation process is not diffusion controlled, probably due to the presence of a homogeneous chemical process.³⁵ The difference between peak potentials for the reduction and oxidation (ΔE_p) is substantially higher than what could be expected for a reversible process.³⁵ The reduction counterpart occurs at -0.21 V vs. SHE with a peak intensity ratio between the reduction and

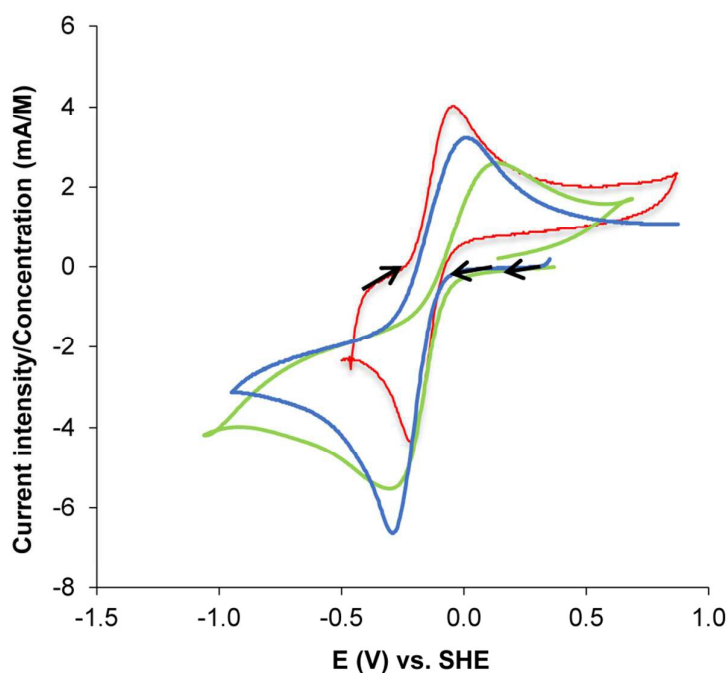


Figure 7 Normalized cyclic voltammograms at 200 mV s^{-1} of complexes **1** (red), **2** (green) and **3a** (blue) in dichloromethane solutions of $[N(n\text{-Bu})_4][\text{BF}_4]$ (0.2 M).

Table 2 Representative redox peaks of complexes **1**, **2** and **3a**. E_p^{ox} and E_p^{red} represent the oxidation and reduction potentials, respectively, in V vs. SHE. Potentials measured at 200 mV s⁻¹.

Complex	E_p^{ox}	E_p^{red}	ΔE_p	$E_{1/2}$
1	-0.03	-0.21	0.18	-0.12
2	0.14	-0.38	0.52	-0.12
3a	0.01	-0.29	0.30	-0.14

oxidation peaks ($i_{p_{red}}/i_{p_{ox}}$) of around 1 and practically independent of the scan rate.

Complex **3a** shows a one electron reduction process at -0.29 V corresponding to the reduction of Co(III) to Co(II) displaying a 1.8 fold increase in the current-function for a 20 fold decrease in the scan rate, indicating that the reduction process is once more not diffusion controlled but is influenced by the presence of a chemical process (Figure S8 of the ESI). The oxidation counterpart occurs at 0.01 vs. SHE with a peak intensity ratio between the reduction and oxidation peaks ($i_{p_{red}}/i_{p_{ox}}$) of around 1.8 practically independent of the scan rate, indicating that only approximately half of the original Co(III) complex that was reduced to Co(II) is again reoxidized back to Co(III). This chemical irreversibility is in accordance with the observed behaviour for the current function with scan rate. The difference between peak potentials for the reduction and oxidation (ΔE_p) is again substantially higher than what is expected for a reversible process.

The homogeneous chemical reaction detected in the electrochemical behaviour of both complexes **1** and **3** could be due to the presence of an isomerization process in solution.³⁶ The presence of an equilibrium in solution between two isomers of both **1** and **3** with slightly different E^0 could be envisaged as a possible explanation for the observed electrochemical behaviour.

The reduction peak potential of **1** shifting towards more anodic potentials with time was also observed, significantly reducing the ΔE_p value. This indicates that a time driven homogeneous reaction is occurring in solution, leading to the more stable isomer, which is responsible for the less negative peak reduction potential. Isomerization processes have been reported and their mechanism investigated for other Co(II) and Co(III) octahedral complexes bearing bidentate chelating ligands.³⁷

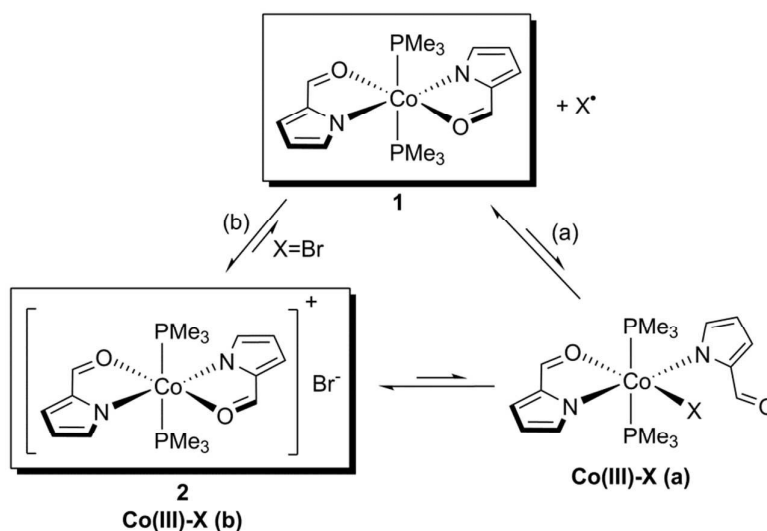
Complex **2** shows a one electron reduction process at -0.38 V vs. SHE corresponding to the reduction of Co(III) to Co(II). The oxidation counterpart occurs at 0.14 V vs. SHE with a peak intensity ratio between the reduction and oxidation peaks ($i_{p_{red}}/i_{p_{ox}}$) increasing considerably with time. The instability of this complex in the time scale of the experiment contrasts with the behaviour of the equivalent Co(III) complex **3a** indicating a possible role of the Br⁻ counter-ion in this process. Initially the ratio of the reduction to the oxidation intensity peak was 1.7 indicating that, as with **3a**, only approximately half of the original Co(III) complex that was reduced to Co(II)

was again reoxidized back to Co(III) complex. The difference between peak potentials for the reduction and oxidation (ΔE_p) is once more substantially higher than what is expected for a reversible process, which again can be explained by the presence of an isomerization process.

In order to understand the possible role of the bromide counter-ion in the electrochemical response of **2**, addition of stoichiometric amounts of $[N(n\text{-Bu})_4][\text{Br}]$ to a solution of **1** in the CV cell caused an immediate shift in the cathodic peak potential of **1** towards anodic potentials, as observed in the evolution with time during the CV study of **1** described above. The bromide ion could be seen as a catalyst that promotes the formation of the supposed more stable isomer form of complex **1**.

Homopolymerizations of styrene and methyl methacrylate mediated by complex 1 – considerations on the nature of the Co(III) mediator species: Taking into account all the aspects discussed above and the mechanisms proposed for the homopolymerizations of Sty (ATRP) and MMA (OMRP/CCT) (see Scheme 1), some considerations of the possible nature of species **Co(III)-Br** and **Co(III)-P_n** can be envisaged.

A possibility could be that, owing to the antibonding nature of the SOMO orbital of the Co-O bond in complex **1** and to the isomerization process detected in the CV studies, which is promoted by the presence of Br^- , the formylpyrrolyl ligands of **1** exhibit a hemilabile behaviour consisting in the decoordination/coordination of the aldehyde arm of the formylpyrrolyl chelate. Considering that the PMe_3 ligands do not undergo a facile dissociation process, the postulated deactivator **Co(III)-X** ($X = \text{Br}$ or P_n) species of Scheme 1 could result from the addition of the



Scheme 3 Possible natures of the **Co(III)-X** ($X = \text{Br}$ or P_n) deactivator species operating in the proposed mechanisms for the homopolymerizations of Sty (ATRP) and MMA (OMRP/CCT) (see Scheme 1).

corresponding radical (halogen radical $\text{Br}\cdot$ or growing radical polymer chain $\text{P}_n\cdot$) to the site liberated by the oxygen atom, resulting in the formal oxidation of **1** (Scheme 3, route a).

Alternatively, one could think that the deactivator species **Co(III)-Br** corresponds to the isolated cationic complex **2** itself, in which the bromine atom is the counteranion. It would then participate in an activator/deactivator equilibrium, via a direct Outer-Sphere Electron Transfer (OSET), occurring between the anion and cation (Scheme 3, route b).

Homopolymerizations of styrene and methyl methacrylate mediated by complex 2 – Single-component system: Following the CV studies, the activity of complexes **2**, **3a** and **3b** was screened in the polymerization of Sty and MMA (Table S3 in ESI). The reactions were conducted in 1,2-dichloroethane due to the insolubility of these cationic complexes in aromatic solvents. Between 50 and 90 °C, for MMA, and 70 and 90 °C, for Sty, complex **2** was active in the respective polymerization reactions, as a single-component initiator system. The system was active for [monomer]:[**2**] ratios as high as 500:1 for Sty and 2000:1 for MMA polymerization, and follows a first order kinetics in relation to the monomers. Although quite active for the MMA polymerization, complex **2** leads to a lower activity when compared with **1/tBiB-Br** mediation and, on the other hand, similar activities for Sty polymerization were observed for both systems. Conversely, a crucial observation is that complexes **3a** and **3b** are not active whatsoever towards the polymerization of those monomers. The homopolymerization reactions mediated by complex **2** were also performed in toluene, however no activity was observed. Figure 8 shows that once the ratio [monomer]:[**2**] increases the reaction rate decreases, as observed for the system mediated by **1/tBiB-Br**. Although these results were quite promising for a single-component system, the control throughout the homopolymerization reactions of MMA and styrene was poor as the molecular weights obtained were much higher than expected. The activity of complex **2**, which contains a potentially coordinating Br^- counter-anion, in contrast with the inactivity exhibited by complexes **3a** and **3b**, containing non-coordinating counter-anions, suggests that Br is somehow operating in the polymerization processes mediated by complex **2**.

The activity of complex **2** towards the polymerization of Sty and MMA can be based on a possible mechanism of Generation of Activators by Monomer Addition (GAMA), reported for some systems mediated by $[\text{FeBr}_3\text{L}_n]$ (where L_n is a phosphorus(III) ligand).³⁸ In the present case, the cobalt atom in complex **2** is already in the highest oxidation state, meaning that Br^- is prone to oxidation to $\text{Br}\cdot$, possibly via an OSET mechanism, leading to the observed polymerization activity (Scheme 3, route b). This type of initiation, involving $\text{Br}\cdot$ as initiator, requires two molecules of

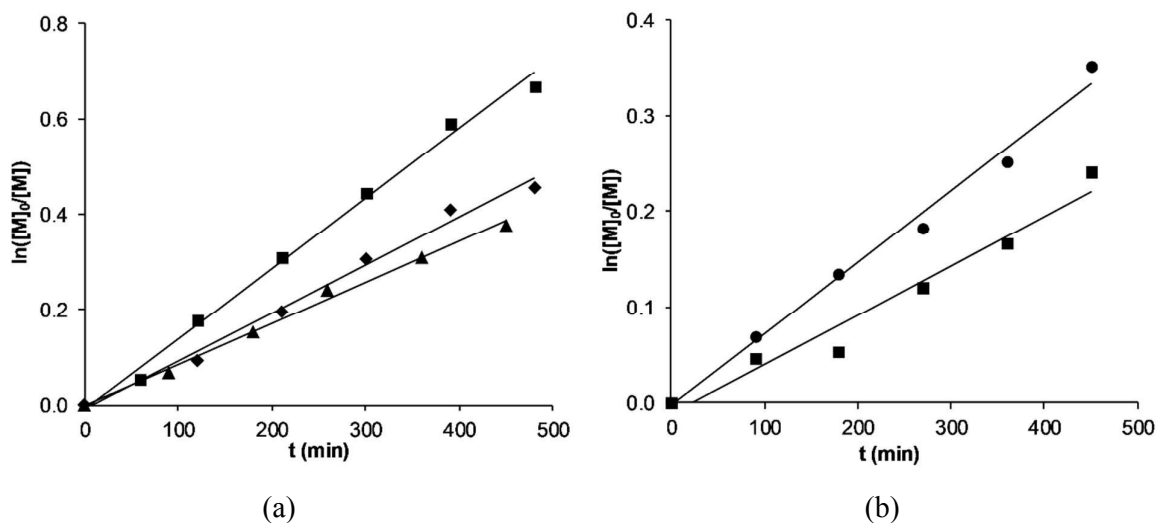


Figure 8 First order kinetic plots ($\ln([M]_0/[M])$ vs. time) for the homopolymerizations of MMA (a) and Sty (b), $[monomer]:[2]$ ratios of 250:1 (circles), 500:1 (squares), 1000:1 (diamonds) and 2000:1 (triangles). Reaction temperature = 70 °C; $V_{monomer}:V_{1,2-dichloroethane} = 5:10$ mL.

complex per polymer chain, which gives rise to polymer molecular weights higher by at least a factor of two in relation to the theoretical living polymerization line.

Homopolymerizations of styrene and methyl methacrylate mediated by complex 2 – Reverse-ATRP conditions: Complex **2** was also tested under reverse-ATRP conditions, by combination with 0.5 equivalents of AIBN, in 1,2-dichloroethane solution, at 70 °C (Table S4 in ESI). In the case of the polymerization of MMA, addition of AIBN to the system led to results similar to those observed when using complex **2** alone as a mediator.

In the case of Sty, significant differences were observed: by using AIBN, the reaction rate increased around 1.5 times and the molecular weight control improved (Figure 9). In fact, the molecular weights observed for the system **2**/AIBN are now only around 1.5 times higher (instead of the 2- to 10-fold increase observed for **2** alone) than the ones predicted by the ideal line. Furthermore, the dispersities (*ca.* 1.5) are lower than before. The improved molecular weight control over Sty polymerization following the addition of AIBN is attributed to the much higher initiation efficiency, in comparison with mediation by **2** alone. In this case, the initiation is due to the organic radicals generated from the thermal decomposition of AIBN, enabling the bromine radicals to act exclusively as atom transfer agents. This leads to an activation/deactivation equilibrium typical of a reverse-ATRP mechanism, since the starting Co(III) complex **2** is in the highest oxidation state. Since the decomposition of AIBN is not quantitative, only a fraction of

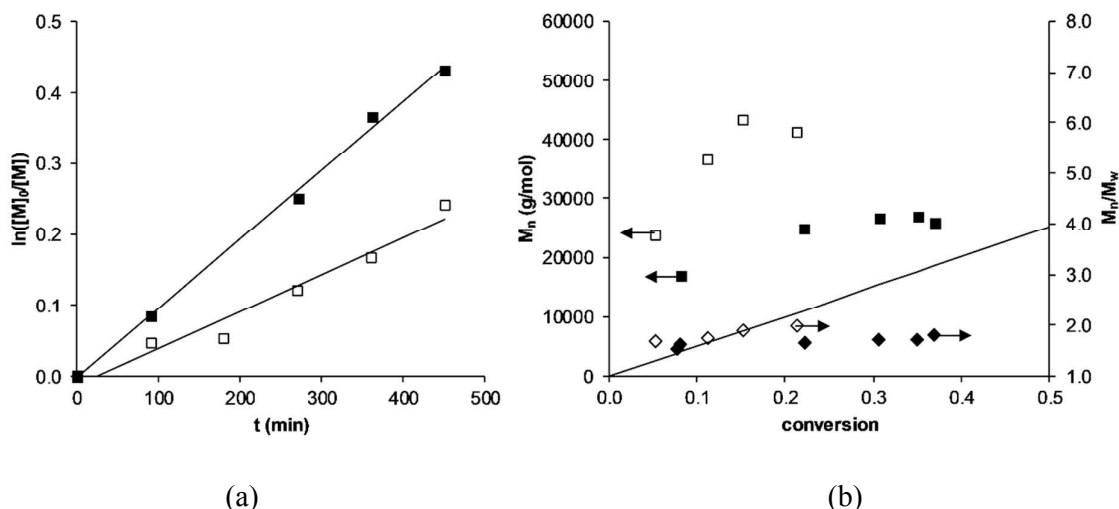


Figure 9 (a) First order kinetic plots ($\ln([M]_0/[M])$ vs. time) for the homopolymerization of Sty mediated with **2** (white squares) and with **2/AIBN** (black squares). (b) Plots of M_n (squares) and \bar{D} (diamonds) vs. conversion of Sty mediated by **2** (white) and by **2/AIBN** (black) (the straight line represents the theoretical living polymerization M_n values).

[Monomer]:[**2**]=500:1 and [Monomer]:[**2**]:[AIBN]=500:1:0.5. Reaction temperature=70 °C;

$V_{\text{monomer}}:V_{1,2\text{-dichloroethane}}=5:5$ mL.

those actually initiate the polymeric chains, leading to slightly higher effective [monomer]:[**2**]:[AIBN] ratios, which result in higher molecular weights.

Conclusions

Under ATRP conditions, the system $[\text{Co}^{\text{III}}\{\kappa^2\text{N,O-NC}_4\text{H}_3\text{-C(H)=O}\}_2(\text{PMe}_3)_2]$ (**1**)/tBiB-Br successfully mediated the RDRP of MMA below 50 °C and Sty below 70 °C. The polymerization of Sty actually occurred via an ATRP mechanism, whereas MMA polymerization favoured an OMRP/CCT interplay mechanism. The bromine termination of the PS formed with this system allowed the formation of the block copolymer PS-*b*-PMMA, as confirmed by GPC/SEC and DOSY NMR experiments.

In an attempt to isolate a Co(III) species containing a Br atom (**Co(III)-Br**), which could be a key ATRP deactivator in this process, the stoichiometric reaction of **1** with tBiB-Br was conducted. The formation of the cationic complex $[\text{Co}^{\text{III}}\{\kappa^2\text{N,O-NC}_4\text{H}_3\text{-C(H)=O}\}_2(\text{PMe}_3)_2]\text{Br}$ (**2**) took place, containing a Br^- counter-anion, from the one-electron oxidation of **1** by tBiB-Br. Metathetical exchange reactions performed with compound **2**, enabled the substitution of the coordinating counter-anion Br^- , by the non-coordinating BF_4^- and $\text{B}(\text{C}_6\text{H}_5)_4^-$ ones, giving rise to complexes **3a** and **3b**, respectively. The formulation of complexes **2**, **3a** and **3b** was confirmed by NMR

spectroscopy and X-ray diffraction. Complexes **1**, **2** and **3a** were studied by cyclic voltammetry, showing quasi-reversible Co(II)/Co(III) redox behaviors, with **1** and **2** exhibiting the same $E_{1/2}$ value and **3a** a more negative one.

Complexes **2**, **3a** and **3b** were screened in the polymerization of Sty and MMA, among which only complex **2** displayed activity as a single-component mediator, likely via a GAMA process, caused by an outer-sphere electron transfer of the Br⁻ counter-anion and subsequent addition of Br⁻ to the monomers, albeit with poor molecular weight control. Under reverse-ATRP conditions, complex **2** (*i.e.* **2**/AIBN) was able to reasonably control the polymerization of styrene at 70 °C, but not that of MMA. However, complexes **3a** and **3b** are completely inactive towards the polymerization of Sty or MMA.

Experimental

General: All operations were performed under dry dinitrogen atmosphere using standard glovebox and Schlenk techniques unless otherwise noted. Solvents were pre-dried with molecular sieves and refluxed under dinitrogen and suitable drying agents (sodium/benzophenone for toluene, diethyl ether and THF; CaH₂ for *n*-hexane, dichloromethane and 1,2-dichloroethane). Sty and MMA were dried over CaH₂ and distilled under reduced pressure at or below room temperature prior to use and stored at -20 °C. Complex **1**,¹ TIBF₄,³⁹ and B(C₆F₅)₃⁴⁰ were prepared as described in the literature. TIBPh₄ was prepared by reaction of NaBPh₄ with Ti₂SO₄. The remaining reagents were purchased and used as received.

Synthesis of [Co{κ²N,O-NC₄H₃-C(H)=O}₂(PMe₃)₂][Br] (2**):** A Schlenk tube charged with **1** (0.4 g, 1 mmol) was dissolved in *ca.* 15 mL of toluene. A toluene solution of tBiB-Br (0.25 g, 1.1 mmol) was added dropwise to the solution of **1** at room temperature. The mixture was stirred for 24 h at 30 °C, during which the yellow-brown solution turned into an orange suspension. The near colourless supernatant liquid was filtered off, the orange solid washed with *n*-hexane and toluene (2 times) and dried under vacuum. The solid was redissolved in dichloromethane, the solution was concentrated and carefully double-layered with a threefold amount of *n*-hexane, and cooled to -20 °C, quantitatively yielding an orange-red microcrystalline solid. Crystals suitable for X-ray diffraction were grown from slow evaporation of a dichloromethane solution in air.

¹H NMR (300 MHz, CD₂Cl₂): δ 7.63 (s, 2H, C(O)H), 7.49 (s, 2H, H₃_{pyrr}), 7.44 (t, 2H, H₄_{pyrr}, ³J_{HH}=3Hz), 6.75 (d, 2H, H₅_{pyrr}, ³J_{HH}=3Hz), 0.85 (t, 18H, P(CH₃)₃, ²J_{HP}=6 Hz). ¹³C{¹H} NMR (75 MHz, CD₂Cl₂): δ 181.0 (C(O)H), 145.8 (C₂_{pyrr}), 145.3 (t, C₅_{pyrr}, ⁴J_{CP}=3.8 Hz), 126.6 (C₄_{pyrr}), 121.5

(t, C3_{pyrr}, ³J_{CP}=3 Hz), 9.56 (t, P(CH₃)₃, ²J_{CP}=13.5 Hz). ³¹P{¹H} NMR (121 MHz, CD₂Cl₂): δ 13.2 (P(CH₃)₃). Anal. Calc. For C₁₆H₂₆BrCoN₂O₂P₂: C, 40.11; H, 5.47; N, 5.85. Found: C, 39.93; H, 5.50; N, 5.64.

Synthesis of [Co{κ²N,O-NC₄H₃-C(H)=O}₂(PMe₃)₂][X] (X=BF₄⁻ (3a**), BPh₄⁻ (**3b**)):** A Schlenk tube was charged with **2** (1 mmol) and dissolved in *ca.* 15 mL of dichloromethane, whereupon TIX (1 mmol) was quickly added as a solid to the solution. The white coarse solid turned into a off-white fine solid. The suspension was stirred for 2 h. The red solution was filtered, the volatiles being removed under reduced pressure, and the residue subsequently washed with *n*-hexane and toluene (2 times). The remaining solid was redissolved in dichloromethane, the solution concentrated and carefully double-layered with a threefold amount of *n*-hexane, and cooled to -20 °C, quantitatively yielding an orange-red microcrystalline solid. Crystals suitable for X-ray diffraction were grown from slow evaporation of a dichloromethane solution in air.

Data for **3a** (X=BF₄⁻): ¹H NMR (300 MHz, CD₂Cl₂): δ 7.56 (s, 2H, C(O)H), 7.51 (s, 2H, H₃_{pyrr}), 7.44 (s, 2H, H₄_{pyrr}, ³J_{HH}=3 Hz), 6.75 (s, 2H, H₅_{pyrr}, ³J_{HH}=3 Hz), 0.85 (t, 18H, P(CH₃)₃, ²J_{HP}=6 Hz). ¹³C{¹H} NMR (75 MHz, CD₂Cl₂): δ 181.0 (C(O)H), 145.9 (C₂_{pyrr}), 145.3 (t, C₅_{pyrr}, ⁴J_{CP}=3.8 Hz), 126.5 (C₄_{pyrr}), 121.6 (t, C₃_{pyrr}, ³J_{CP}=3 Hz), 8.94 (t, P(CH₃)₃, ²J_{CP}=13.5 Hz). ³¹P{¹H} NMR (121 MHz, CD₂Cl₂): δ 12.7 (P(CH₃)₃). ¹⁹F{¹H} NMR (282 MHz, CD₂Cl₂): δ -152.6 (BF₄⁻). ¹¹B{¹H} NMR (96 MHz, CD₂Cl₂): δ -1.2 (BF₄⁻). Anal. Calc. For C₁₆H₂₆BCoF₄N₂O₂P₂: C, 39.54; H, 5.39; N, 5.76. Found: C, 39.67; H, 5.52; N, 5.51.

Data for **3b** (X=BPh₄⁻): ¹H NMR (300 MHz, CD₂Cl₂): δ 7.48 (s, 2H, C(O)H), 7.39 (s, 2H, H₃_{pyrr}), 7.33 (br, 9H, H_{ortho}(BPh₄⁻) + H₄_{pyrr}), 7.03 (t, 8H, H_{meta}(BPh₄⁻), ³J_{HH}=2.3 Hz), 6.89 (t, 4H, H_{para}(BPh₄⁻), ³J_{HH}=3 Hz), 6.76 (d, 2H, H₅_{pyrr}, ³J_{HH}=1.5 Hz), 0.78 (t, 18H, P(CH₃)₃, ²J_{HP}=6 Hz). ¹³C{¹H} NMR (75 MHz, CD₂Cl₂): δ 180.5 (C(O)H), 164.5 (q, C_{ipso}(BPh₄⁻), ¹J_{CB}=48.8 Hz), 145.8 (C₂_{pyrr}), 145.4 (t, C₅_{pyrr}, ⁴J_{CP}=3.8 Hz), 136.5 (q, C_{ortho}(BPh₄⁻), ²J_{CB}=3 Hz), 125.9 (q, C_{meta}(BPh₄⁻), ³J_{CB}=3 Hz), 122.3 (s, C_{para}(BPh₄⁻)), 121.9 (t, C₃_{pyrr}, ³J_{CP}=3 Hz), 8.42 (t, P(CH₃)₃, ²J_{CP}=13.5 Hz). ³¹P{¹H} NMR (121 MHz, CD₂Cl₂): δ 12.5 (P(CH₃)₃). ¹¹B{¹H} NMR (96 MHz, CD₂Cl₂): δ -6.6 (BPh₄⁻). Anal. Calc. For C₄₀H₄₆BCoN₂O₂P₂: C, 66.87; H, 6.45; N, 3.90. Found: C, 66.88; H, 6.61; N, 4.01.

Generation of [Co{κ²N,O-NC₄H₃-C(H)=O}₂(PMe₃)₂][BrB(C₆F₅)₃] (4**):** Complex **2** (20 mg, 0.0417 mmol) and B(C₆F₅)₃ (21.4 mg, 0.0417 mmol) were dissolved in CD₂Cl₂ and placed in a J-Young NMR tube. After 2 h, the NMR spectra were acquired, confirming the formation of complex **4** in a near quantitative yield.

^1H NMR (300 MHz, CD_2Cl_2): δ 7.47 (br, 4H, $\text{C}(\text{O})\text{H} + \text{H}_{3\text{pyrr}}$), 7.39 (br, 2H, $\text{H}_{4\text{pyrr}}$), 6.74 (br, 2H, $\text{H}_{5\text{pyrr}}$), 0.80 (t, 18H, $\text{P}(\text{CH}_3)_3$, $^2\text{J}_{\text{HP}}=6$ Hz). $^{31}\text{P}\{^1\text{H}\}$ NMR (121 MHz, CD_2Cl_2): δ 12.4 ($\text{P}(\text{CH}_3)_3$). $^{11}\text{B}\{^1\text{H}\}$ NMR (96 MHz, CD_2Cl_2): δ -0.1 ($[\text{BrB}(\text{C}_6\text{F}_5)_3]^-$). $^{19}\text{F}\{^1\text{H}\}$ NMR (282 MHz, CD_2Cl_2): δ -130.7 (d, 2F, $\text{F}_{\text{ortho}}(\text{BC}_6\text{F}_5)$, $^3\text{J}_{\text{CF}}=19.7$ Hz), -159.2 (br, 1F, $\text{F}_{\text{para}}(\text{BC}_6\text{F}_5)$), -166.05 (t, 2F, $\text{F}_{\text{meta}}(\text{BC}_6\text{F}_5)$, $^3\text{J}_{\text{CF}}=21.5$ Hz).

General procedure for homopolymerization reactions: The appropriate mass of metal complex was weighed (typically 0.090 mmol) under dinitrogen atmosphere to a degassed Schlenk tube, which was subsequently charged with the reaction solvent (typically 4 mL) and a solution of tBiB-Br (typically 0.090 mmol of initiator in 1 mL of solvent), for ATRP experiments, or solid AIBN (typically 0.045 mmol), for reverse-ATRP experiments. The mixture was placed in a thermostated oil bath (for experiments between 50 and 90 °C) or in a thermostated water bath (for experiments at 25 °C) set at the desired temperature. The monomer (typically 45 mmol) was then added quickly to the previous mixture, defining the start of the reaction. Aliquots of the reaction mixture (1 mL) were periodically withdrawn and precipitated in excess of methanol (*ca.* 10 times). The solid was filtered off, washed with methanol and dried under vacuum until constant weight. The conversion of monomer for each of the periodically withdrawn aliquots was calculated by dividing the obtained polymer mass found in each aliquot by the initial mass of monomer existing in each aliquot (1 mL). All the samples were analysed by GPC/SEC and selected samples were analysed by NMR spectroscopy.

Synthesis of the block-copolymer PS-*b*-PMMA from PS-Br: Using the same procedure described above, the polymerization of styrene was carried out at 50 °C and at a [monomer]:[1]:[tBiB-Br] molar ratio of 500:1:1. After 24 h of reaction, the reaction mixture was dissolved in THF and passed through a dried silica column (Aldrich), under nitrogen, in order to try to retain the residual metal complex. The resulting solution was evaporated to dryness, stored in a degassed Schlenk tube and dried under vacuum, 0.821 g of a brownish solid being obtained. The molecular weight of the solid was determined by GPC/SEC. 0.041 g of complex **1** (0.10 mmol) and 0.57 g of the polystyryl bromide solid were transferred to a degassed Schlenk tube. The solid mixture was dissolved in 5.5 mL of toluene. 5.5 mL of methyl methacrylate (52 mmol) were added to the previous solution and the mixture was thermostated at 50 °C ([monomer]:[1]:[tBiB-Br]=500:1:1). Aliquots (1 mL) were withdrawn periodically and, after workup, analysed by GPC/SEC, and some of them by NMR. The conversion of monomer for each of the periodically

withdrawn aliquots was calculated by dividing the obtained polymer mass found in each aliquot by the initial mass of MMA existing in each aliquot (1 mL).

NMR measurements: The NMR spectra of complexes, as well as those of PS and PMMA homopolymers, were recorded on a *Bruker "AVANCE III"* 300 MHz spectrometer at 299.995 MHz (^1H), 75.4296 MHz (^{13}C), 121.439 MHz (^{31}P), 282.218 MHz (^{19}F) and 96.2712 MHz (^{11}B), and referenced in general to the residual protio- and carbon resonances of the corresponding solvents (for ^1H and ^{13}C spectra, respectively). The NMR spectra of the PS samples in 1,1,2,2-tetrachloroethane- d_2 were performed at 120 °C. The NMR spectra of the PMMA samples in CDCl_3 were performed at 55 °C. The NMR spectra of the PS-*b*-PMMA block-copolymer in 1,1,2,2-tetrachloroethane- d_2 , were recorded on a *Bruker "AVANCE III"* 500 MHz spectrometer equipped with a 5 mm BBO probe, at 70 °C, and referenced to the proton or carbon resonances of hexadimethylsiloxane (HDMSO) (δ 0.06 for ^1H , and δ 2.0 for ^{13}C). The DOSY spectrum was obtained at 25 °C using a bipolar stimulated echo sequence (STE) with smoothed square gradients. All the solution samples were prepared in dried and degassed deuterated solvents at room temperature, using standard 5 mm NMR tubes. For air/moisture sensitive compounds, the samples were prepared in a glovebox in J. Young NMR tubes.

Molecular weight measurements: GPC/SEC analysis were performed by eluting THF solutions of the polymeric samples at 35 °C (Waters oven) in two PolyPore columns (protected by a PolyPore guard column) (Polymer Labs) mounted on a Waters 1515 isocratic HPLC pump. The detection was performed by a Waters 2414 differential refractive index detector. The THF eluent was filtered through 0.45 μm PTFE Pall membrane filters and degassed in an ultrasound bath. Solution samples were filtered through 0.20 μm PTFE GVS filters. The system was calibrated with TSK Tosoh Co. polystyrene standards.

MALDI-TOF mass spectrometry (MALDI-TOF MS): MALDI-TOF MS analyses were performed by the Laboratório de Análises da FCT-UNL, Monte da Caparica, Portugal, in a time-of-flight mass spectrometer Voyager-DETM PRO Workstation, using the MALDI ionization technique, with analysis by a positive reflector. For the PMMA samples, a matrix of DHB+ NaBF_4 was used and for the polystyrene samples, a matrix of ditranol+ AgOOCCF_3 was used. The ionization of the polystyrenes was unsuccessful.

X-ray diffraction: Crystallographic and experimental details of crystal structure determinations are listed in Table 2. The crystals were selected in air, covered with polyfluoroether oil and mounted on a nylon loop. Crystallographic data were collected using graphite monochromated Mo-K α radiation ($\lambda=0.71073$ Å) on a Bruker AXS-KAPPA APEX II diffractometer equipped with an Oxford Cryosystem open-flow nitrogen cryostat, at 150 K. Cell parameters were retrieved using Bruker SMART⁴¹ software and refined using Bruker SAINT⁴² on all observed reflections. Absorption corrections were applied using SADABS.⁴³ Structure solution and refinement were performed using direct methods with the programs SIR2004⁴⁴ and SHELXL-2018/1⁴⁵ included in the package of programs WINGX-Version 2014.1.⁴⁶ When analysing the data of **2**, a value of $|E^2-1| = 0.676$ was found, pointing to the presence of twinning in the crystal. Therefore, refinement as a 2-component inversion twin was performed, and the BASF components refined equally to 0.37(2). All hydrogen atoms were inserted in idealised positions and allowed to refine riding on the parent carbon atom. All the structures refined to a perfect convergence. Graphic presentations were prepared with ORTEP-III^{46b,47} and Mercury 3.9.⁴⁸ Data was deposited in CCDC under the deposit numbers 1574383 for **2**, 1574384 for **3a** and 1574385 for **3b**.

Cyclic voltammetry measurements: Cyclic voltammetry experiments on 3 mM solutions of complexes **1**, **2** and **3a** in dichloromethane, using [N(*n*-Bu)₄][BF₄] (0.2 M) as a supporting electrolyte, were performed at a scanning rate of 200 mV s⁻¹ with a three compartment electrochemical cell, under nitrogen atmosphere, at room temperature, using a Pt disc working electrode and a Pt wire counter electrode, with a Ag pseudo-reference electrode connected to the main compartment by a Luggin capillary. The redox potentials were calculated using the reference potential of the ferrocene/ferrocenium couple.

Acknowledgements

We thank the Fundação para a Ciência e a Tecnologia, Portugal, for financial support (Project UID/QUI/00100/2013) and for fellowships to T.F.C.C. and C.S.B.G., (PD/BD/52372/2013-CATSUS PhD programme and SFRH/BPD/107834/2015, respectively).

References

- 1 K. Matyjaszewski, *Macromolecules*, 2012, **45**, 4015–4039.

- 2 W. A. Braunecker, K. Matyjaszewski, *Prog. Polym. Sci.*, 2007, **32**, 93–146.
- 3 R. P. N. Veregin, P. G. Odell, L. M. Michalak, M. K. Georges, *Macromolecules*, 1996, **29**, 4161–4163.
- 4 J.-S. Wang, K. Matyjaszewski, *Macromolecules*, 1995, **28**, 7901–7910.
- 5 K. Matyjaszewski, J. Xia, *Chem. Rev.*, 2001, **101**, 2921–2990.
- 6 L. E. N. Allan, M. R. Perry, M. P. Shaver, *Prog. Polym. Sci.*, 2012, **37**, 127–156.
- 7 B. B. Wayland, G. Poszmik, M. Fryd, *Organometallics*, 1992, **14**, 3534–3542.
- 8 For example: (a) A. Debuigne, R. Poli, C. Jérôme, R. Jérôme, C. Detrembleur, *Prog. Polym. Sci.*, 2009, **34**, 211–239; (b) K. M. Smith, W. S. McNeil, A. S. Abd-El-Aziz, *Macromol. Chem. Phys.*, 2010, **211**, 10-16; (c) M. Hurtgen, C. Detrembleur, C. Jerome, A. Debuigne, *Polym. Rev.* 2011, **51**, 188–213; (d) K. Matyjaszewski, M. Möller, *Polymer Science: A Comprehensive Reference*, 2012, Vol. 3, 351–375; (e) A. Debuigne, C. Jérôme, C. Detrembleur, *Polymer* 2017, **115**, 285–307.
- 9 (a) M. P. Shaver, L. E. N. Allan, H. S. Rzepa, V. C. Gibson, *Angew. Chem. Int. Ed.*, 2006, **45**, 1241–1244; (b) R. Poli, M. P. Shaver, *Chem. Eur. J.*, 2014, **20**, 17530–17540.
- 10 A. Gridnev, *J. Polym. Sci. Part A Polym. Chem.*, 2000, **38**, 1753–1766.
- 11 A. Debuigne, R. Poli, C. Jérôme, R. Jérôme, C. Detrembleur, *Prog. Polym. Sci.*, 2009, **34**, 211–239.
- 12 R. Poli, *Angew. Chem. Int. Ed.*, 2006, **45**, 5058–5070.
- 13 R. Banerjee, S. W. Ragsdale, *Annu. Rev. Biochem.*, 2003, **72**, 209–247.
- 14 B. B. Wayland, G. Poszmik, S. L. Mukerjee, M. Fryd, *J. Am. Chem. Soc.*, 1994, **116**, 7943–7944.
- 15 R. Poli, *Chem. Eur. J.*, 2015, **21**, 6988–7001.
- 16 C.-H. Peng, M. Fryd, B. B. Wayland, *Macromolecules*, 2007, **40**, 6814–6819.
- 17 K. S. Santhosh Kumar, Y. Li, Y. Gnanou, U. Baisch, Y. Champouret, R. Poli, K. C. D. Robson, W. S. McNeil, *Chem. Asian J.*, 2009, **4**, 1257–1265.
- 18 S. Maria, H. Kaneyoshi, K. Matyjaszewski, R. Poli, *Chem. Eur. J.*, 2007, **13**, 2480–2492.
- 19 U. Baisch, R. Poli, *Polyhedron*, 2008, **27**, 2175–2185.
- 20 A. Debuigne, Y. Champouret, R. Jérôme, R. Poli, C. Detrembleur, *Chem. Eur. J.*, 2008, **14**, 4046–4059.
- 21 A. Debuigne, C. Michaux, C. Jérôme, R. Jérôme, R. Poli, C. Detrembleur, *Chem. Eur. J.*, 2008, **14**, 7623–7637.

- 22 (a) A. Debuigne, A. N. Morin, A. Kermagoret, Y. Piette, C. Detrembleur, C. Jérôme, R. Poli, *Chem. Eur. J.*, 2012, **18**, 12834–12844; (b) A. N. Morin, C. Detrembleur, C. Jérôme, P. De Tullio, R. Poli, A. Debuigne, *Macromolecules*, 2013, **46**, 4303–4312.
- 23 B. Wang, Y. Zhuang, X. Luo, S. Xu, X. Zhou, *Macromolecules*, 2003, **36**, 9684–9686.
- 24 (a) S. A. Carabineiro, L. C. Silva, P. T. Gomes, L. C. J. Pereira, L. F. Veiros, S. I. Pascu, M. T. Duarte, S. Namorado, R. T. Henriques, *Inorg. Chem.*, 2007, **46**, 6880–6890; (b) S. A. Carabineiro, R. M. Bellabarba, P. T. Gomes, S. I. Pascu, L. F. Veiros, C. Freire, L. C. J. Pereira, R. T. Henriques, M. C. Oliveira, J. E. Warren, *Inorg. Chem.*, 2008, **47**, 8896–8911; (c) C. S. B. Gomes, S. A. Carabineiro, P. T. Gomes, M. T. Duarte, *Inorg. Chim. Acta*, 2011, **367**, 151–157; (d) C. S. B. Gomes, M. T. Duarte, P. T. Gomes, *J. Organomet. Chem.*, 2014, **760**, 167–176.
- 25 S. A. Carabineiro, P. T. Gomes, L. F. Veiros, C. Freire, L. C. J. Pereira, R. T. Henriques, J. E. Warren, S. I. Pascu, *Dalton Trans.*, 2007, **46**, 5460–5470.
- 26 J.-F. Lutz, K. Matyjaszewski, *J. Polym. Sci. Part A Polym. Chem.*, 2005, **43**, 897–910.
- 27 K. Matsuzaki, T. Uryu, T. Asakura, *NMR Spectroscopy and Stereoregularity of Polymers*, Japan Scientific Societies Press and S. Karger; Tokyo and Basel, 1996, , Chapter 4, p. 57.
- 28 K. Hatada, T. Kitayama, K. Ute, Y. Terawaki, T. Yanagida, *Macromolecules*, 1997, **30**, 6754–6759.
- 29 (a) M. H. C. Byrd, S. A. Bencherif, B. J. Bauer, K. L. Beers, Y. Brun, S. Lin-Gibson, N. Sari, *Macromolecules*, 2005, **38**, 1564–1572; (b) M. Mitchell, *Synthetic Approaches to Novel Highly Functionalized Polythiophenes*, M.Sc. Thesis., Iowa State University, 2007 (<http://lib.dr.iastate.edu/cgi/viewcontent.cgi?article=15866&context=rtd>; last accessed in 31/10/2017).
- 30 E. Le Grogneq, J. Claverie, R. Poli, *J. Am. Chem. Soc.*, 2001, **123**, 9513–9524.
- 31 P. A. Chase, M. Parvez, W. E. Piers, *Acta Cryst.*, 2006, **E62**, 5181–5183.
- 32 R. H. Crabtree, *The Organometallic Chemistry of the Transition Metals*; John Wiley & Sons, 2014, Chapter 10, p. 260.
- 33 C. Jablonski, Z. Zhou, J. Bridson, *Inorg. Chim. Acta*, 1997, **254**, 315–328.
- 34 G. R. Eaton, *J. Chem. Educ.*, 1969, **46**, 547–556.
- 35 A. J. Bard, L. R. Faulkner, *Electrochemical Methods: Fundamentals and Applications*, 2nd Ed., Wiley, 2000.

- 36 A. Pombeiro, M. F. C. G. Silva, M. A. N. D. A. Lemos, *Coord. Chem. Rev.*, 2001, **219–221**, 53–80
- 37 (a) F. Riblet, G. Novitchi, R. Scopelliti, L. Helm, A. Gulea, A. E. Merbach, *Inorg. Chem.*, 2010, **49**, 4194–4211; (b) W. R. Fitzgerald, D. W. Watts, *J. Am. Chem. Soc.*, 1967, **89**, 821–824.
- 38 For example: (a) Z. Xue, D. He, S. K. Noh, W. S. Lyoo, *Macromolecules*, 2009, **42**, 2949–2957; (b) D. He, Z. Xue, M. Y. Khan, S. K. Noh, W. S. Lyoo, *J. Polym. Sci. Part A: Polym. Chem.*, 2010, **48**, 144–151; (c) Z. Xue, N. T. B. Linh, S. K. Noh, W. S. Lyoo, *Angew. Chem. Int. Ed.*, 2008, **47**, 6426–6429; (d) Z. Xue, H. S. Oh, S. K. Noh, W. S. Lyoo, *Macromol. Rapid Commun.*, 2008, **29**, 1887–1894.
- 39 F. J. Arnáiz, *J. Chem. Educ.*, 1997, **74**, 1332–1333.
- 40 (a) A. N. Chernega, A. J. Graham, M. L. H. Green, J. Haggitt, J. Lloyd, C. P. Mehnert, N. Metzler, J. Souter, Dalton Trans., J. Chem. Soc., *Dalton Trans.*, 1997, 2293–2303; (b) D. S. Lancaster, *ChemSpider Synthetic Pages*, 2003, 215.
- 41 SMART Software for the CCD Detector System Version 5.625, Bruker AXS Inc., Madison, WI, USA, 2001.
- 42 SAINT Software for the CCD Detector System, Version 7.03, Bruker AXS Inc., Madison, WI, USA, 2004.
- 43 G.M. Sheldrick, SADABS, Program for Empirical Absorption Correction, University of Göttingen, Göttingen, 1996.
- 44 M. C. Burla, R. Caliandro, M. Camalli, B. Carrozzini, G. L. Cascarano, L. De Caro, C. Giacovazzo, G. Polidori, R. Spagna, *J. Appl. Crystallogr.*, 2005, **38**, 381–388.
- 45 (a) SHELXL: G. M. Sheldrick, *Acta Crystallogr., Sect. C: Struct. Chem.*, 2015, **71**, 3–8; (b) C. B. Hübschle, G. M. Sheldrick and B. Dittrich, ShelXle: a Qt graphical user interface for SHELXL, *J. Appl. Crystallogr.*, 2011, **44**, 1281–1284.
- 46 (a) L. J. Farrugia, *J. Appl. Crystallogr.*, 1999, **32**, 837–838; (b) L. J. Farrugia, *J. Appl. Crystallogr.*, 2012, **45**, 849–854.
- 47 (a) M. N. Burnett, C. K. Johnson, ORTEP-III: Oak Ridge Thermal Ellipsoid Plot Program for Crystal Structure Illustration, Oak Ridge National Laboratory, 1996. Report ORNL-6895.
(b) ORTEP3 for Windows - L. J. Farrugia, *J. Appl. Crystallogr.*, 1997, **30**, 565.
- 48 C. F. Macrae, P. R. Edgington, P. McCabe, E. Pidcock, G. P. Shields, R. Taylor, M. Towler and J. van de Streek, *J. Appl. Crystallogr.*, 2006, **39**, 453–457.

Table of Contents entry

Bis(formylpyrrolyl) cobalt complexes mediate the Reversible-Deactivation Radical Polymerization of styrene and methyl methacrylate

